Relationship between particle and heat transport in JT-60U plasmas with internal transport barrier

H. Takenaga 1), S. Higashijima 1), N. Oyama 1), L. G. Bruskin 1), Y. Koide 1), S. Ide 1), H. Shirai 1), Y. Sakamoto 1), T. Suzuki 1), K. W. Hill 2), G. Rewoldt 2), G. J. Kramer 2), R. Nazikian 2), T. Takizuka 1), T. Fujita 1), A. Sakasai 1), Y. Kamada 1), H. Kubo 1) and the JT-60 Team 1)

1) Japan Atomic Energy Research Institute, Naka Fusion Research Establishment, Naka-machi, Naka-gun, Ibaraki-ken, 311-0193, Japan
2) Princeton Plasma Physics Laboratory, Princeton, New Jersey, 08543-0451, U.S.A.

e-mail contact of main author : takenaga@naka.jaeri.go.jp

Abstract. The relationship between particle and heat transport in an internal transport barrier (ITB) has been systematically investigated in reversed shear (RS) and high β_p ELMy H-mode plasmas in JT-60U. No helium and carbon accumulation inside the ITB is observed even with ion heat transport reduced to a neoclassical level. On the other hand, the heavy impurity argon is accumulated inside the ITB. The argon density profile estimated from the soft x-ray profile is more peaked, by a factor of 2-4 in the RS plasma and of 1.6 in the high β_p mode plasma, than the electron density profile. The helium diffusivity (D_{He}) and the ion thermal diffusivity (χ_i) are at an anomalous level in the high β_p mode plasma, where D_{He} and χ_i are higher by a factor of 5-10 than the neoclassical value. In the RS plasma, D_{He} is reduced from the anomalous to the neoclassical level, together with χ_i. The carbon and argon density profiles calculated using the transport coefficients reduced to the neoclassical level only in the ITB are more peaked than the measured profiles, even when χ_i is reduced to the neoclassical level. Argon exhaust from the inside of the ITB is demonstrated by applying ECH in the high β_p mode plasma, where both electron and argon density profiles become flatter. The reduction of the neoclassical inward velocity for argon due to the reduction of density gradient is consistent with the experimental observation. In the RS plasma, the density gradient is not decreased by ECH and argon is not exhausted. These results suggest the importance of density gradient control to suppress heavy impurity accumulation.

1. Introduction

A reversed or weak positive magnetic shear plasma with internal transport barriers (ITBs) is a most promising operation mode for advanced steady-state operation due to its high bootstrap current fraction and high confinement. In JT-60U, the reversed shear (RS) plasma and the high β_p mode plasma with weak positive shear have been optimized to provide a physics basis for ITER and SSTR [1]. In these plasmas, further optimization for high density, high radiation loss fraction and high fuel purity are necessary, as well as high β while keeping high confinement. Since these issues are closely related to the particle transport, understanding of the relationship between particle and heat transport is indispensable for the optimization.

In this paper, the relationship between particle (i.e., electron, helium, carbon and argon) and heat transport is systematically investigated in the high β_p mode and RS plasmas. In the high β_p mode plasma, anomalous transport is dominant. On the other hand, in the RS plasma, ion heat transport is reduced from the anomalous to the neoclassical level. The characteristics of particle and heat transport at the ITB are discussed in Sec. 2. In Sec. 3, the ITB controllability is studied, followed by a summary in Sec. 4.

2. Characteristics of particle and heat transport at internal transport barrier

Typical profiles of temperatures (T_e, T_i), safety factor (q), and densities (n_e, n_{He}, n_C and n_{Ar}) are shown in Fig. 1 for (a) the RS plasma (I_p=1.3 MA, B_T=3.7 T, R~3.3 m, a~0.8 m, κ~1.5, δ=0.18-0.26 and HH_{y2}~1.6) and (b) the high β_p ELMy H-mode plasma (I_p=1.0 MA, B_T=2-3.8 T, R~3.4 m, a~0.8 m, κ~1.4, δ=0.38-0.46 and HH_{y2}~1.0). The puffed He and intrinsic C densities are measured with CXRS. The profile of the total Ar density summed over all ionization states is estimated using an impurity transport code, where the transport coefficient

is determined by fitting the calculated soft x-ray profile to the measurement [2]. The Ar radiation coefficient is taken from the ADAS database [3] considering the JT-60U diagnostic setup. In the RS plasma, a box-type profile with a strong ITB is observed in $n_e(r)$, $T_e(r)$ and $T_i(r)$. An ITB is also observed in $n_{He}(r)$. However, $n_{He}(r)$ is flatter than $n_e(r)$, which is favorable for helium ash exhaust. The $n_C(r)$ shape is similar to that for $n_e(r)$, suggesting no carbon accumulation inside the ITB. In the RS plasma with a small amount of Ar puffing, the soft x-ray profile becomes a peaked one. In order to fit the calculated soft x-ray profile to the measurement, a more peaked (by a factor of 2.6) $n_{Ar}(r)$ inside the ITB than $n_e(r)$ is necessary, as shown in Fig. 1 (a). This result indicates the Ar accumulation inside the ITB. In the high β_p mode plasma, $n_e(r)$, $T_e(r)$ and $T_i(r)$ have a parabolic-type profile. Both $n_{He}(r)$ and $n_C(r)$ are flat, also suggesting no helium and carbon accumulation. On the other hand, $n_{Ar}(r)$ is more peaked by a factor of 1.6 than $n_e(r)$, which is, however, a smaller factor than that in the RS plasma.

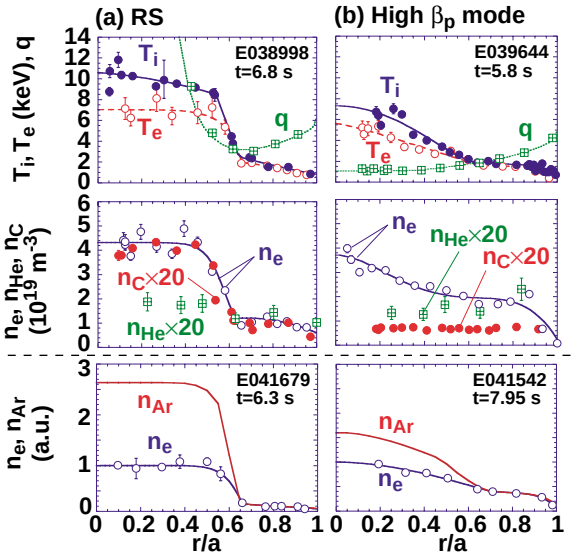

Fig. 1 Profiles of temperatures, safety factor, and densities of electrons, He, C and Ar in (a) RS and (b) high β_p mode plasmas. In the bottom figures, $n_e(r)$ is normalized at r/a=0 and $n_{Ar}(r)$ is adjusted to $n_e(r)$ outside the ITB.

Figure 2 shows $(-\nabla n/n)$ as a function of $(-\nabla T_i/T_i)$ for n_e, n_{He}, n_C and n_{Ar} at the ITB. In the high β_p mode plasma, $(-\nabla n/n)$ and $(-\nabla T_i/T_i)$ are limited to small values compared with those in the RS plasma. Although the error range is large due to scattering of the measured n_{He}, $(-\nabla n_{He}/n_{He})$ has a negative value. The value of $(-\nabla n_C/n_C)$ is around zero, and is smaller than $(-\nabla n_e/n_e)$. Due to the Ar accumulation, $(-\nabla n_{Ar}/n_{Ar})$ is larger than $(-\nabla n_e/n_e)$. On the other hand, in the RS plasma, $(-\nabla n_e/n_e)$ increases with $(-\nabla T_i/T_i)$ from the same region as that for the high β_p mode plasma, and it is similar to $(-\nabla T_i/T_i)$. The value of $(-\nabla n_{He}/n_{He})$ is saturated in the range of large $(-\nabla T_i/T_i)$, and it is smaller than $(-\nabla n_e/n_e)$. When He is fuelled inside the ITB using a He beam, $(-\nabla n_{He}/n_{He})$ is larger than that with He gas-puffing. However, even with the He beam, $(-\nabla n_{He}/n_{He})$ is still smaller than $(-\nabla n_e/n_e)$. The value of $(-\nabla n_C/n_C)$ is almost the same as $(-\nabla n_e/n_e)$, and $(-\nabla n_{Ar}/n_{Ar})$ is larger than $(-\nabla n_e/n_e)$ due to the Ar accumulation. The higher Z impurity has larger $(-\nabla n/n)$ in the RS plasma.

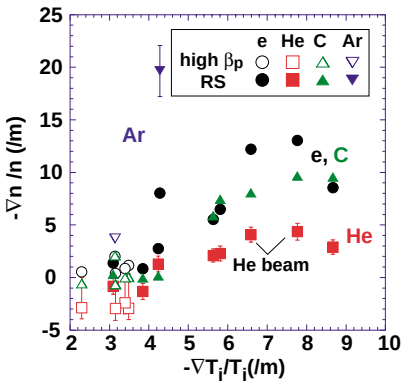

Fig. 2 Relationship between $(-\nabla n/n)$ and $(-\nabla T_i / T_i)$ for n_e, n_{He}, n_C and n_{Ar}. Open and closed symbols show the data in the high β_p mode and RS plasmas, respectively.

Next, the relationship between particle and thermal diffusivities is discussed. The electron effective diffusivity (D_e^{eff}), defined considering only the diffusion term, is well correlated with the ion thermal diffusivity (χ_i) in both high β_p mode and RS plasmas. The ratio (D_e^{eff}/χ_i) is estimated to be 0.2-0.3 in the high β_p mode plasma and 0.04-0.2 in the RS plasma. In order to understand the relationship, the heat and particle fluxes are estimated based on the linear stability analysis using the FULL code [4] in the box-type RS plasma. The FULL code analysis indicates that a positive linear growth rate still remains at the ITB region even with sheared E×B rotation effects. The 2D full wave code analysis [5] also shows the existence of 0.5-2% density fluctuations around the ITB based on O-mode reflectometer measurement [6]. The FULL code estimates the ratio of particle flux to the electron heat flux ($\Gamma_e T_e/q_e$) to be

around unity in the ITB region, and the ratio drops to a value just slightly negative outside the ITB. Although the experimental profile of the ratio decreases much smoothly from around unity in the ITB region to about 0.1 outside the ITB, it shows a similar tendency. The ratio of ion anomalous heat flux to electron heat flux (q_i^a/q_e) has a similar value (q_i^a/q_e =5-7) for both experiment and calculation outside the ITB. However, in the ITB region, q_i^a/q_e for the calculation is much smaller than that for the experiment. A possible reason for the disagreement is that the FULL code analysis represents the linear limit with a single value of $k_\theta\rho_i$ based on a local theory. The non-linear effects, the effects summed over all values of $k_\theta\rho_i$ and non-local effects should be investigated to understand physical mechanisms responsible for the relationship between particle and heat transport.

The relationship between the impurity diffusivity normalized by the neoclassical value (D/D^{NC}) and χ_i/χ_i^{NC} in the ITB is shown in Fig. 3. The values of D and the convection velocity (v) of He are estimated separately based on the He gas-puffing modulation experiment [7]. Since it is difficult to separate D and v for C and Ar experimentally, D_C and D_{Ar} are estimated by assuming the neoclassical v (v^{NC}) and a steady-state condition. In the RS plasma, a similar v to the neoclassical value has been obtained for C and Ne [8, 9]. The impurity neoclassical transport coefficient is calculated using NCLASS [10]. The value of D_{He} is estimated to be 0.5-1.0 m^2/s in the high β_p mode plasma and 0.1-0.5 m^2/s in the RS plasma. The ratio D_{He}/χ_i is in the range of 0.2-1.0 for both RS and high β_p mode plasmas. The value of D_{He} is reduced to the neoclassical level in the box-type RS plasma, where χ_i is also reduced to the neoclassical value. In the parabolic-type RS plasma and high β_p mode plasma, D_{He} and χ_i are higher by a factor of 5-10 than D_{He}^{NC} and χ_i^{NC}. The value of v is consistent with the neoclassical theory (from ~0 to –1.3 m/s) in not only box-type but also parabolic-type RS plasmas. On the other hand, an outward v is observed in the high β_p mode plasma, while the neoclassical theory predicts a small inward v. The outward v is consistent with the negative value of ($-\nabla n_{He}/n_{He}$) shown in Fig. 2.

The values of D_C^{NC} and D_{Ar}^{NC} are estimated to be in the range 0.01-0.04 m^2/s at the ITB. The value of v^{NC} at the ITB is larger for Ar (-0.2 to -0.8 m/s in the high β_p mode plasma and -2 to -5 m/s in the RS plasma) than for C (~0 to -0.2 m/s in the high β_p mode plasma and ~0 to -1.3 m/s in the RS plasma). The steady-state $n_C(r)$ and $n_{Ar}(r)$ calculated using $D=D^{NC}$ at ITB and D=1 m^2/s in the other region with v^{NC} are more peaked than the measurements, even in the box-type RS plasma. Although the experimental $n_C(r)$ and $n_{Ar}(r)$ is not in steady state in the box-type RS plasma, the experimental $n_C(r)$ and $n_{Ar}(r)$ is not as peaked as the neoclassical prediction even when time evolution is considered. In order to adjust the calculated steady-state profile to the measurement with v^{NC}, larger D_C and D_{Ar} are necessary in the ITB region. In the box-type RS plasma, where χ_i is reduced to the neoclassical level, D_C/D_C^{NC} and D_{Ar}/D_{Ar}^{NC} are estimated to be ~4 and ~9, respectively. The values of D_C and D_{Ar} are estimated to be 0.1 and 0.2 m^2/s, respectively. These values are similar to the range of D_{He} (0.1-0.3 m^2/s). In the high β_p mode plasma, D_C and D_{Ar} are estimated to be about 0.1 m^2/s. The values of D_C/D_C^{NC} and D_{Ar}/D_{Ar}^{NC} are about 4, which is similar to χ_i/χ_i^{NC}=5. In some high χ_i/χ_i^{NC} cases in the parabolic-type RS plasma, D_C/D_C^{NC} is estimated to be more than 10. However, in other high χ_i/χ_i^{NC} cases, $n_C(r)$ can not be reproduced with v^{NC}, because a zero or negative gradient of $n_C(r)$ is observed, although v^{NC} is inward. The anomalous v might be dominant in this region.

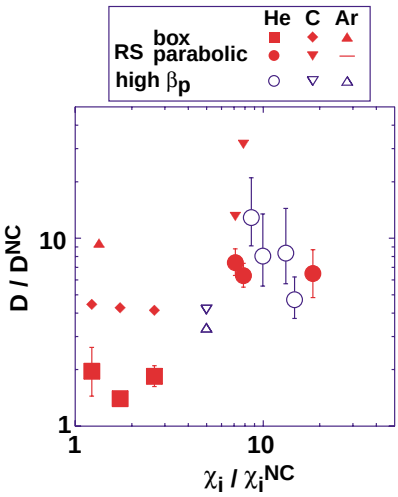

Fig. 3 Relationship between D_{He}/D_{He}^{NC} and χ_i/χ_i^{NC}. Open circles show the data in high β_p mode plasma. Closed circles and squares show the data in parabolic- and box-type RS plasmas, respectively. D_C/D_C^{NC} and D_{Ar}/D_{Ar}^{NC} are also plotted, which are estimated by assuming v^{NC}.

3. Control of internal transport barrier

Although the accumulation is smaller than the neoclassical prediction, the Ar accumulation inside the ITB should be suppressed. In order to control the Ar accumulation inside the ITB, ECH is applied. The density clamp by ECH is a common phenomenon not only in tokamaks

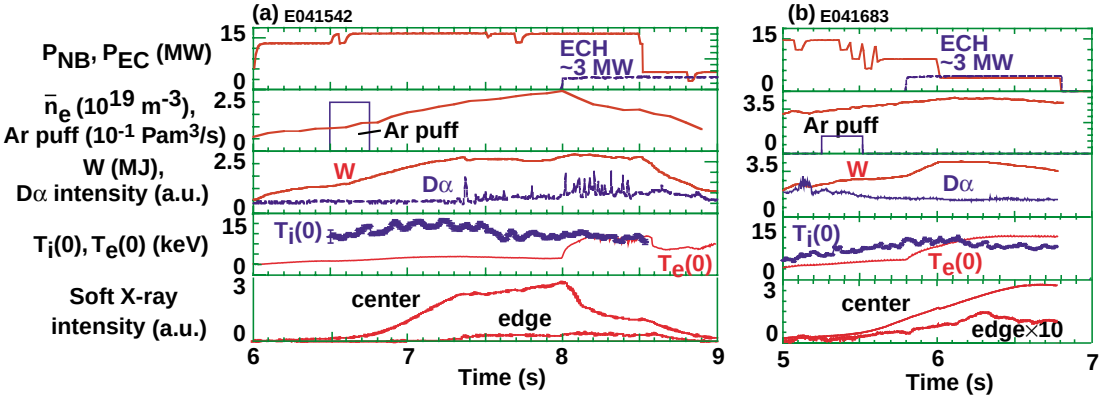

Fig. 4 Wave-forms in (a) high β_p mode and (b) RS plasmas with central ECH and Ar puffing.

but also in helical devices [11, 12]. In addition, a decrease of T_i in the ITB is observed in JT-60U high β_p mode plasma [13]. Figure 4 (a) shows the time evolution of the high β_p mode plasma, where a small amount of Ar was puffed at t=6.5 s and ECH was applied inside the ITB from t=8 s. The value of $T_e(0)$ is increased to the same value as $T_i(0)$ during ECH. The density is substantially decreased by applying ECH while maintaining $T_i(0)$. In a similar discharge without Ar puffing, a decrease of T_i is observed during ECH with small change of n_e. Ar could affect the large reduction of n_e during ECH. Although the thermal confinement is decreased from HH_{y2}=1.0 at t=7.95 s to 0.9 at t=8.45 s, the central soft x-ray signal is drastically reduced by a factor of more than 2. This observation indicates the Ar exhaust from the inside of the ITB. In the RS plasma with Ar puffing, ECH was also applied from t=5.8 s as shown in Fig. 4 (b), where NB power was decreased from t=6.0 s. The confinement is improved by applying ECH until the NB power is decreased. After the NB power is stepped down, the particle fuelling becomes small, but the density does not substantially decrease. The stored energy gradually decreases and HH_{y2} is estimated to be 1.6 at t=6.5 s. The strong ITBs in $n_e(r)$ and $T_i(r)$ remain and the soft x-ray signal does not decrease even after the NB power is stepped down, suggesting no Ar exhaust from the inside of the ITB.

Figure 5 (a) and (b) show $n_e(r)$ and $T_i(r)$, respectively, before and during ECH in the high β_p mode plasma. The n_e ITB is almost lost, while the T_i ITB is kept, although the ITB position moves inward. The decrease of the density gradient leads to the reduction of v^{NC} as shown in Fig. 5 (c). The value of D_{Ar}^{NC} during ECH is almost the same as that before ECH. Figure 5 (d) shows $n_{Ar}(r)$ reproduced using a different v^{NC} and the diffusivity of $D=4\times D_{Ar}^{NC}$ in the ITB and D=0.5-1 m^2/s in the other region. A value of $n_{Ar}(0)$ is substantially reduced compared with $n_e(0)$. These profiles are consistent with the

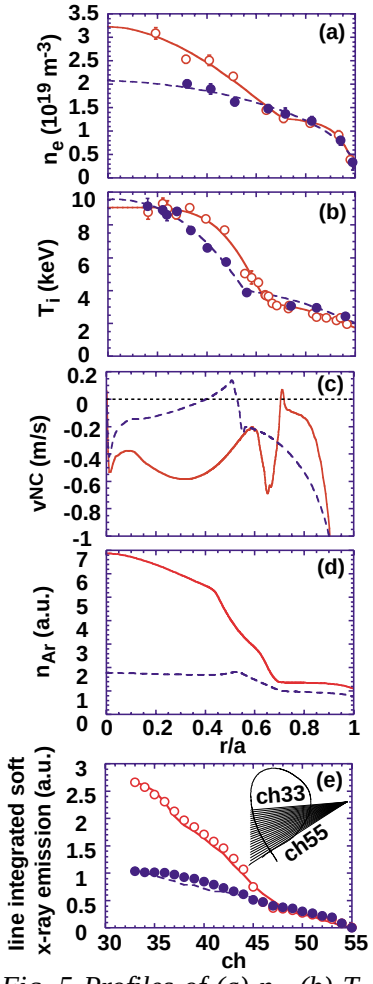

Fig. 5 Profiles of (a) n_e, (b) T_i, (c) v^{NC}, (d) calculated n_{Ar} and (e) calculated (lines) and measured (symbols) soft x-ray profile before (open symbols and solid line) and during (closed symbols and dashed line) ECH in the high β_p mode plasma.

soft x-ray measurements both before and during ECH as shown in Fig. 5 (e). A possible mechanism for the Ar exhaust is as follows. First, the density is clamped by ECH and the density gradient becomes small. Then, Ar is exhausted due to the reduction of v^{NC}. Also, the Ar exhaust reduces the density. These processes could interact as a positive feed back loop for Ar exhaust. These results indicate the importance of the density gradient control to suppress the argon accumulation. In the RS plasma, $n_e(r)$ is not changed and $n_{Ar}(r)$ is still more peaked by a factor of 3-4 than $n_e(r)$ during ECH. This result suggests that there is no Ar exhaust by ECH in the RS plasma. The development of the density gradient control method in the RS plasma is crucial for suppression of Ar accumulation.

The possibility of density gradient control in the RS plasma is shown with pellet injection. When a high field side pellet is injected into the box-type RS plasma, a clear reduction of density fluctuations is observed. The 2D full wave code shows that the fluctuation level is reduced from 1.3% to 0.8%, assuming $k_\theta=k_r=3$ cm^{-1}. The dependence of the density fluctuation level on k_θ and k_r is checked using an analytical solution of the time-dependent 2D full-wave equation [14]. The density fluctuation level before the pellet injection varies in the range 0.8-1.8% by changing k_θ and k_r=1-5 cm^{-1}. The ion temperature profiles are not substantially different before and after the reduction of the density fluctuations. While, the density increases inside the ITB and the density gradient becomes large in the ITB region. The value of $n_C(0)$ is also increased. In this discharge, a cold pulse induced by pellet ablation outside the ITB is propagated into the ITB, and the density fluctuations are reduced. Conversely, local heating outside the ITB might work for the reduction of the density gradient.

4. Summary

The relationship between particle and heat transport is systematically investigated at the ITB in reversed shear and high β_p mode plasmas. The value of $(-\nabla n/n)$ is smaller than $(-\nabla T_i/T_i)$ for helium, similar for electrons and carbon, and larger for argon, in the RS plasma with a box-type profile. The value of D_{He} is reduced to a neoclassical level together with χ_i. On the other hand, 4-9 times larger carbon and argon diffusivities than the neoclassical value are evaluated, even when χ_i is reduced to the neoclassical level. Ar is exhausted from the inside of the ITB by applying ECH in the high β_p mode plasma, while thermal confinement is reduced from HH_{y2}=1.0 to 0.9. In the RS plasma, the electron density profile is not changed and argon is not exhausted by ECH. These results indicate that density gradient control is important in suppressing impurity accumulation inside the ITB.

Acknowledgement

The authors wish to thank Dr. R. Dux for calculating the soft x-ray emission rate of argon and Dr. W. A. Houlberg for use of the NCLASS.

References

[1] KIKUCHI, M., Nucl. Fusion **30** (1990) 265.
[2] KUBO, H., et al., accepted in J. Nucl. Mater.
[3] SUMMERS, H. P., JET-IR 06, JET Joint Undertaking, Culham (1994).
[4] REWOLDT, G., et al., Nucl. Fusion **42** (2002) 403.
[5] VALEO, E. J., et al., Plasma Phys. Control. Fusion **44** (2002) L1.
[6] OYAMA, N., et al., Rev. Sci. Instrum. **73** (2002) 1169.
[7] TAKENAGA, H., et al., Nucl. Fusion **39** (1999) 1917.
[8] TAKENAGA, H., et al., Phys. Plasmas **8** (2001) 2217.
[9] TAKENAGA, H., et al., Fusion Science and Technology **42** (2002) 327.
[10] HOULBERG, W. A., et al., Phys. Plasmas **4** (1997) 3230.
[11] LA HAYE, R. J., et al., Nucl. Fusion **21** (1981) 1425.
[12] ZUSHI, H., et al., Nucl. Fusion **28** (1988) 1801.
[13] IDE, S., et al., IAEA-CN-94/EX/C3-3, this conference.
[14] BRUSKIN, L. G., et al., accepted in Plasma Phys. Control. Fusion.